

A BOUNDARY-LAYER PRECONDITIONER FOR SINGULARLY PERTURBED CONVECTION DIFFUSION*

SCOTT P. MACLACHLAN[†], NIALL MADDEN[‡], AND THÁI ANH NHAN[§]

Abstract. Motivated by a wide range of real-world problems whose solutions exhibit boundary and interior layers, the numerical analysis of discretizations of singularly perturbed differential equations is an established sub-discipline within the study of the numerical approximation of solutions to differential equations. Consequently, much is known about how to accurately and stably discretize such equations on *a priori* adapted meshes, in order to properly resolve the layer structure present in their continuum solutions. However, despite being a key step in the numerical simulation process, much less is known about the efficient and accurate solution of the linear systems of equations corresponding to these discretizations.

In this paper, we discuss problems associated with the application of direct solvers to these discretizations, and we propose a preconditioning strategy that is tuned to the matrix structure induced by using layer-adapted meshes for convection-diffusion equations, proving a strong condition-number bound on the preconditioned system in one spatial dimension, and a weaker bound in two spatial dimensions. Numerical results confirm the efficiency of the resulting preconditioners in one and two dimensions, with time-to-solution of less than one second for representative problems on 1024×1024 meshes and up to $40\times$ speedup over standard sparse direct solvers.

Key words. Singularly Perturbed Differential Equations; Stable Finite-Difference Discretization; Preconditioning; Domain Decomposition; Multigrid Methods

AMS subject classifications. 65F08, 65N22, 65N55

1. Introduction. We are interested in the design and implementation of efficient linear solvers for discretizations of singularly perturbed problems of the form

$$(1.1) \quad -\varepsilon u'' - c(x)u' + r(x)u = f \text{ on } (0, 1),$$

and

$$(1.2) \quad -\varepsilon \Delta u - \mathbf{c}(x, y) \cdot \nabla u + r(x, y)u = f \text{ on } (0, 1)^2,$$

subject to homogeneous Dirichlet boundary conditions. Here, $\varepsilon \in (0, 1]$ is referred to as the “perturbation parameter”; in the cases of primary interest, $\varepsilon \ll 1$. For smooth forcing functions, f , the behaviour of the solution, u , is known to be different for the reaction-diffusion case (with $c = 0$ or $\mathbf{c} = \mathbf{0}$) and the convection-diffusion case (with $c \neq 0$ or $\mathbf{c} \neq \mathbf{0}$). As a result, different discretizations and solver approaches may be appropriate and effective in the two cases. Here, we focus on the convection-diffusion case; a similar strategy for reaction-diffusion problems was previously proposed and analysed in [13], although we note that, as usual, the non-symmetric case requires much different techniques than the symmetric and positive-definite one considered therein.

*Submitted to the editors DATE.

Funding: The work of S.M. was partially funded by an NSERC Discovery Grant. The authors wish to acknowledge the Irish Centre for High-End Computing (ICHEC) for the provision of computational facilities and support.

[†]Department of Mathematics and Statistics, Memorial University of Newfoundland, St. John’s, NL A1C 5S7, Canada (smaclachlan@mun.ca).

[‡]School of Mathematical and Statistical Sciences, National University of Ireland, Galway, Ireland (Niall.Madden@NUIGalway.ie)

[§]Department of Mathematics and Science, Holy Names University, 3500 Mountain Blvd., Oakland, CA 94619, USA (nhan@hnu.edu)

Equations such as (1.1) and (1.2) and their many variants are common in mathematical modelling since their solutions exhibit boundary and/or interior layers. For example, Morton lists ten typical problems which feature equations of these types, including models of water and atmospheric pollution, electric currents in semi-conductors, turbulent transport, and financial derivatives [17, Chap 1.]. Finite-difference methods, and upwind schemes in particular, have long been used for their discretization [10, Chap 10].

In the context of singularly perturbed problems, the challenge for numerical analysts is, usually, to design implementable methods that resolve any layers present and guarantee a certain order of convergence with respect to the mesh size, independent of ε . Methods with such a property are referred to as “parameter robust”. Typically, they are specialist methods involving highly non-uniform meshes, often combined with nonstandard discretizations [1, 11]. The crux of the issue, for all singularly perturbed problems, is that the layers are the regions of greatest interest, but they are located in very narrow regions, with widths that may be as small as $\mathcal{O}(\varepsilon)$. Thus, resolution of these layers with uniform grids would require a mesh resolution is $\mathcal{O}(\varepsilon)$. This is not possible as $\varepsilon \rightarrow 0$. Standard adaptive mesh refinement techniques, such as h - and p -refinement also fail to be robust, since many levels of refinement are needed to resolve the layer regions when starting from a uniform mesh. Thus, a common approach is to use *a priori* adapted meshes that are chosen to resolve the (known) layer regions [12].

A further complication is introduced for convection-dominated problems such as those above: it is well understood that classical methods, such as central finite-difference methods, yield highly oscillatory numerical solutions unless, again, mesh resolution is $\mathcal{O}(\varepsilon)$ [22, 24]. That is, even if one were only interested in qualitatively accurate solutions away from the layers, one still needs an infeasibly large number of degrees of freedom.

The solution to this is to use stabilized discretizations along with layer-adapted grids. In this setting, there are many different approaches for constructing stable discretizations. We will focus on the simplest, and, arguably, most commonly used: upwind finite-difference methods. There are many proposed layer adapted meshes in the literature (see, e.g., [12]). For our exposition, we focus on the most widely studied: the piecewise uniform mesh of Shishkin [16]. However, the analysis extends immediately to more general layer-adapted meshes; see Remark 2.7.

There is a rich mathematical theory underpinning the parameter robustness of upwind finite-difference methods on layer adapted meshes. However, almost exclusively, this work ignores the issue of solving the resulting linear systems. This is an oversight, since it is known that standard direct solvers are surprisingly inefficient when applied to these discretizations [13, 18]. Furthermore, the convergence of standard iterative methods deteriorates drastically as $\varepsilon \rightarrow 0$, unless specialized preconditioning is employed.

The numerical solution of the linear systems resulting from the upwind finite-difference discretization of these problems was first considered in [21], where it was shown that the condition number of the one-dimensional problem discretized on Shishkin meshes with N points scales like $\mathcal{O}(N^2/(\varepsilon \ln^2(N)))$, but that a diagonal preconditioning can be defined to improve this to $\mathcal{O}(N^2/\ln(N))$. Similarly, the performance of Gauss-Seidel for the one-dimensional problem was considered in [8], while numerical experiments for the two-dimensional problem with Incomplete LU preconditioners were performed in [3]. More robust preconditioning strategies have also been considered. In particular, [14] consider an overlapping multiplicative Schwarz

method for the one-dimensional problem, with *volumetric overlap* (meaning the overlap between two subdomains has positive volume), building on existing work showing that this gives parameter-robust solution of the corresponding continuous Schwarz method [15]. They prove convergence of the corresponding discrete Schwarz algorithm as well, and demonstrate robustness of their technique both with respect to the singular perturbation parameter and the mesh size, using exact solves of the resulting subdomain systems.

More recently, [7] proposed a multiplicative-Schwarz preconditioner for the one-dimensional model with *minimal overlap* (meaning that adjacent subdomains share only a single mesh point), again with exact subdomain solves. This results in a rank-one spectral structure for the iteration matrix that allows a full convergence analysis, but precludes extension of these results to two-dimensional models. Robust solution methods based on multigrid principles have also been considered, with [9] considering the two-dimensional model using a standard multigrid approach for anisotropic differential operators, based on full coarsening multigrid with rediscrretization determining coarse-grid operators. In this approach, the inter-grid transfer operators must be adapted, in order to account for the Shishkin mesh structure, and alternating line Gauss-Seidel relaxation is used to account for the resulting anisotropy.

The present work is distinguished by a number of features, though most prominently the development of a special boundary-layer preconditioner, which proposes distinct treatment of the different regions that are induced when using tensor-product layer-adapted meshes. This is in the spirit of the preconditioner proposed in [13] for a reaction-diffusion problem, but is entirely different in implementation and analysis. The complications are due both to the non-symmetric discretization matrices, and the fact that, in two dimensions, the mesh has corner-layer regions where the mesh spacing in the x - and y -directions may, or may not, be highly anisotropic. This work is also distinguished by combining thorough analysis of the preconditioner in one dimension, with a detailed development of an efficient preconditioner for two distinct two-dimensional cases, with supporting heuristics.

Outline. This article is organized as follows. We consider a one-dimensional problem in Section 2. The upwind finite-difference method, and layer-adapted Shishkin mesh, are described in Sections 2.1 and 2.2, respectively. In Section 2.3, we propose an idealized preconditioner for this problem, and provide a detailed analysis in Section 2.4, culminating in proven ε -robust bounds on the spectrum of the preconditioned system. We conclude the study of the one-dimensional problem in Section 2.5 with a presentation of numerical results verifying the uniform convergence of the difference scheme, a discussion on a suitable stopping criterion for GMRES, and iteration counts for preconditioned GMRES, showing the effectiveness of the strategy as $\varepsilon \rightarrow 0$.

Section 3 is devoted to two-dimensional problems. The solutions to such equations can be very different in their nature; depending on c in (1.2), they may possess intersecting layers that are both exponential in nature, or a mixture of exponential and parabolic in nature. We describe the meshes and discretizations for both these cases. In Section 3.1, we present the construction of a suitable preconditioner for both cases, focusing on the (coarse) interior region and anisotropic edge-layer regions, and examining the convergence rate when an idealized preconditioner is used in the corner region. The practical task of preconditioning the corner region, with a multigrid approach, is discussed at length in Section 3.2. In Section 3.3, we present results for two test problems, showing the robust convergence of the scheme, the scaling of the solving times with N and ε , the robustness of the iteration counts with respect to N and ε , and the speedup achieved over a best-in-class direct solver. Conclusions and

remarks on potential future work are given in Section 4.

2. The one-dimensional problem. Recall the one-dimensional problem (1.1), subject to the boundary conditions $u(0) = u(1) = 0$. We shall assume that

$$(2.1) \quad 0 < \underline{C} \leq c(x) \leq \overline{C} \quad \text{and} \quad 0 \leq r(x) \quad \text{for all } x \in [0, 1].$$

2.1. Discretization. We first introduce the (for now, arbitrary) mesh $\Omega^N := \{0 = x_0 < x_1 < \dots < x_N = 1\}$. We use the notation $c_i := c(x_i)$, $r_i := r(x_i)$, $h_i = x_i - x_{i-1}$, and $\bar{h}_i = (h_i + h_{i+1})/2$.

The standard (centred) second-order finite-difference scheme on this mesh has as its stencil, at mesh point i ,

$$(2.2) \quad \left[-\frac{\varepsilon}{h_i \bar{h}_i} + \frac{c_i}{2\bar{h}_i}, \frac{\varepsilon}{\bar{h}_i} \left(\frac{1}{h_i} + \frac{1}{h_{i+1}} \right) + r_i, -\frac{\varepsilon}{h_{i+1} \bar{h}_i} - \frac{c_i}{2\bar{h}_i} \right].$$

Although this scheme is formally second-order (at least on uniform meshes), it is well known (see, e.g., [24, Remark 3.1]) that it usually leads to highly oscillatory solutions when applied on a uniform mesh. Various explanations are possible. Here, we note that the scheme associated with (2.2) cannot yield oscillatory solutions if the matrix is an M-matrix [4], which will be the case if it is diagonally dominant and has its only positive entries on the diagonal. However, it is clear that the subdiagonal entry is non-positive only when $\varepsilon \geq c_i h_i/2$. For arbitrarily small ε , generating a discretization matrix that is an M-matrix would, thus, require that h_i be $\mathcal{O}(\varepsilon)$ for each i . Since that is not a reasonable requirement, an upwind finite-difference method is preferred, even though it is formally of lower order. Its stencil, at mesh point i , is

$$(2.3) \quad \left[-\frac{\varepsilon}{h_i \bar{h}_i}, \frac{\varepsilon}{\bar{h}_i} \left(\frac{1}{h_i} + \frac{1}{h_{i+1}} \right) + \frac{c_i}{h_{i+1}} + r_i, -\frac{\varepsilon}{h_{i+1} \bar{h}_i} - \frac{c_i}{h_{i+1}} \right].$$

Although this scheme is only first-order, its system matrix is an M-matrix for any ε and mesh, and solutions cannot feature spurious oscillations on any mesh.

2.2. Boundary layer fitted meshes. One can apply the scheme in (2.3) on a uniform mesh to solve (1.1) numerically, and, at mesh points, the computed solution will be quantitatively and qualitatively reasonable. However, layers present in the true solution to (1.1) will not be resolved and, consequently, the global error (e.g., between any polynomial interpolant of the numerical solution and the true solution of (1.1)) will be $\mathcal{O}(1)$. The simplest remedy for this is to use a specially constructed *layer-adapted mesh* [12]. There are numerous varieties of these, but they share the same basic construction: in the layer region (whose location is determined *a priori* using qualitative analysis techniques), the mesh is very fine, while elsewhere it is coarse and uniform.

We focus here on the much studied *Shishkin mesh* [16]. For (1.1), subject to the assumptions in (2.1), we define a *mesh transition point*

$$(2.4) \quad \tau = \min \left\{ \frac{1}{2}, \frac{2\varepsilon}{\underline{C}} \ln(N) \right\}.$$

Then the mesh is constructed by forming uniform grids with $N/2$ intervals on each of the subdomains $[0, \tau]$ and $[\tau, 1]$; see Figure 2.1. Then, if u is the solution of (1.1) evaluated at the mesh points, and U^E denotes the solution computed on this mesh using the upwind scheme of (2.3), it can be proven that

$$(2.5) \quad \|u - U^E\|_\infty \leq CN^{-1} \ln N,$$

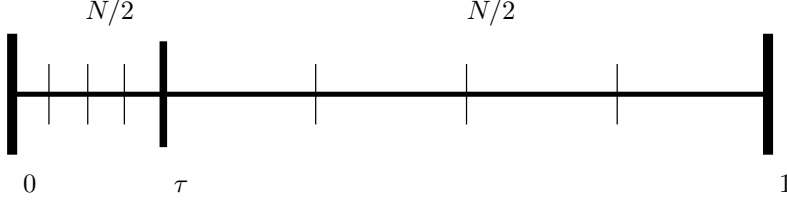


FIG. 2.1. Sketch of a Shishkin mesh for the one-dimensional problem (1.1)

where the constant C is independent of N and ε ; see, e.g., [24, Thm. 3.39].

Remark 2.1. Linß [12, p10] provides a more general construction of a Shishkin mesh for this problem, introducing a parameter q that determines the proportion of mesh points in the layer. Specifically, taking q so that qN is an integer, one modifies (2.4) so that $\tau = \min \{q, 2\varepsilon/C \ln(N)\}$. Then, one forms uniform grids on the subdomains $[0, \tau]$ and $[\tau, 1]$ so that they have qN and $(1 - q)N$ intervals, respectively. In Section 2.5, we take the standard choice of $q = 1/2$; however, in the following section, we develop the preconditioner for a mesh with arbitrarily many mesh points in the layer and interior regions.

2.3. The preconditioner. Consider the one-dimensional problem in (1.1), discretized to give the stencil in (2.3) on a Shishkin mesh. Within the layer, $h_i \approx \varepsilon/N$ (discarding the $\ln(N)$ factor for simplicity of presentation), so the stencil can be approximated by

$$\left[-\frac{N^2}{\varepsilon}, 2\frac{N^2}{\varepsilon} + \frac{c_i N}{\varepsilon} + r_i, -\frac{N^2}{\varepsilon} - \frac{c_i N}{\varepsilon} \right],$$

and we see that both the left- and right-side connections are significant, with the diffusion terms dominating in the limit of large N (regardless of the value of ε). In contrast, in the interior region, $h_i \approx 1/N$, so the stencil is approximately

$$[-\varepsilon N^2, 2\varepsilon N^2 + c_i N + r_i, -\varepsilon N^2 - c_i N].$$

When $\varepsilon N \ll 1$, the $\mathcal{O}(1)$ convection coefficient dominates the diffusion coefficient, resulting in a system that is dominated by its upper bidiagonal part, with the entry on the subdiagonal being comparatively negligible.

Motivated by the above, we consider a block partitioning of the system matrix, A , and associated discrete vectors, into regions where the meshwidths are $\mathcal{O}(\varepsilon/N)$ (typically near layers, so denoted by L), and those where the meshwidths are $\mathcal{O}(1/N)$ (typically in the domain's interior, so denoted by I). We include the transition point in the mesh (with an interval with $\mathcal{O}(\varepsilon/N)$ meshwidth to its left and $\mathcal{O}(1/N)$ to its right) in L , the layer set. In this notation,

$$(2.6) \quad A = \begin{bmatrix} A_{LL} & A_{LI} \\ A_{IL} & A_{II} \end{bmatrix},$$

where A is an $N \times N$ matrix, A_{LL} is an $N_L \times N_L$ matrix, and A_{II} being an $N_I \times N_I$ matrix, with $N = N_L + N_I$. From above, we see that we can accurately approximate the action of A_{II} by its upper triangular part (including the diagonal), M_{II} , leading to a block-structured preconditioner for A , given as

$$(2.7) \quad M = \begin{bmatrix} A_{LL} & A_{LI} \\ A_{IL} & M_{II} \end{bmatrix}.$$

This can be viewed in several ways, including as a type of Schwarz iteration where we are, simply, using an inexact subdomain solve on the interior region of the mesh (noting that A_{IL} has only a single nonzero entry, in its first row and last column).

2.4. Theory. Schwarz methods for this problem have been considered before, in [7, 14]. For one-dimensional problems, with tridiagonal discretization matrices, the spectral structure of the error-propagation operators often has very tractable form; however, this may limit the applicability of the resulting preconditioners to one-dimensional problems, if the resulting methods rely on this special structure. As we show below, the intuition behind the block-structured preconditioner in (2.7) generalizes more readily. The analysis of the eigenvalues of the preconditioned system, however, is somewhat more involved. We begin by characterizing the eigenvalues of $M^{-1}A$ based on the matrix structure, using the notation $\mathbf{e}^{(k)}$ for the canonical unit vector of length N , with all entries equal to zero except the k^{th} , which is equal to one.

THEOREM 2.2. *Let $S_A = A_{II} - A_{IL}A_{LL}^{-1}A_{LI}$ and $S_M = M_{II} - A_{IL}A_{LL}^{-1}A_{LI}$. Then $M^{-1}A$ has (at least) N_L eigenvalues equal to 1, with eigenvectors $\mathbf{e}^{(k)}$ for $1 \leq k \leq N_L$. The other N_I eigenvalues are the eigenvalues of $S_M^{-1}S_A$.*

Proof. From the block structure, we can block factorize both A and M as

$$A = \begin{bmatrix} I & 0 \\ A_{IL}A_{LL}^{-1} & I \end{bmatrix} \begin{bmatrix} A_{LL} & 0 \\ 0 & S_A \end{bmatrix} \begin{bmatrix} I & A_{LL}^{-1}A_{LI} \\ 0 & I \end{bmatrix},$$

$$M = \begin{bmatrix} I & 0 \\ A_{IL}A_{LL}^{-1} & I \end{bmatrix} \begin{bmatrix} A_{LL} & 0 \\ 0 & S_M \end{bmatrix} \begin{bmatrix} I & A_{LL}^{-1}A_{LI} \\ 0 & I \end{bmatrix},$$

where I is understood to be the suitably sized identity matrix. By direct calculation, we then have

$$M^{-1}A = \begin{bmatrix} I & A_{LL}^{-1}A_{LI} \\ 0 & I \end{bmatrix}^{-1} \begin{bmatrix} I & 0 \\ 0 & S_M^{-1}S_A \end{bmatrix} \begin{bmatrix} I & A_{LL}^{-1}A_{LI} \\ 0 & I \end{bmatrix},$$

which we recognize as a similarity transformation of the block-diagonal matrix

$$\begin{bmatrix} I & 0 \\ 0 & S_M^{-1}S_A \end{bmatrix}.$$

Thus, $M^{-1}A$ has the same eigenvalues as this matrix, giving (at least) N_L eigenvalues equal to one, and the remaining eigenvalues as those of $S_M^{-1}S_A$. That the unit eigenvalues have eigenvectors $\mathbf{e}^{(k)}$ for $1 \leq k \leq N_L$ follows from the fact that $A\mathbf{e}^{(k)} = M\mathbf{e}^{(k)}$ for $1 \leq k \leq N_L$. \square

Computing the eigenvalues of $S_M^{-1}S_A$ is the harder task. To do this, we first explicitly compute $A_{IL}A_{LL}^{-1}A_{LI}$, exploiting the fact that both A_{IL} and A_{LI} have only a single nonzero entry, due to the tridiagonal structure of A . Noting that, from the block structure,

$$(A_{LI})_{i,j} = a_{i,N_L+j} \text{ for } 1 \leq i \leq N_L, 1 \leq j \leq N_I,$$

$$(A_{IL})_{i,j} = a_{N_L+i,j} \text{ for } 1 \leq i \leq N_I, 1 \leq j \leq N_L,$$

we can recognize that only $(A_{LI})_{N_L,1}$ and $(A_{IL})_{1,N_L}$ are nonzero, and we can write

$$A_{LI} = a_{N_L,N_L+1} \hat{\mathbf{e}}^{(N_L)} \left(\hat{\mathbf{e}}^{(1)} \right)^T,$$

$$A_{IL} = a_{N_L+1,N_L} \hat{\mathbf{e}}^{(1)} \left(\hat{\mathbf{e}}^{(N_L)} \right)^T,$$

where $\hat{e}^{(1)}$ denotes the first canonical unit vector of length N_I and $\hat{e}^{(N_L)}$ denotes the last canonical unit vector of length N_L . Then, from direct calculation, we have

$$\begin{aligned} A_{IL}A_{LL}^{-1}A_{LI} &= \left(a_{N_L+1,N_L} \hat{e}^{(1)} \left(\hat{e}^{(N_L)} \right)^T \right) A_{LL}^{-1} \left(a_{N_L,N_L+1} \hat{e}^{(N_L)} \left(\hat{e}^{(1)} \right)^T \right) \\ &= a_{N_L+1,N_L} a_{N_L,N_L+1} (A_{LL}^{-1})_{N_L,N_L} \hat{e}^{(1)} \left(\hat{e}^{(1)} \right)^T. \end{aligned}$$

Two general results now enable us to estimate how large of a change this term represents in S_M and S_A .

LEMMA 2.3. *Let $A = LU$ be the LU factorization of the $n \times n$ matrix, A , with unit diagonal on L . Then $(A^{-1})_{n,n} = (u_{n,n})^{-1}$.*

Proof. Note that $(A^{-1})_{n,n}$ is naturally expressed as the final entry in the vector $A^{-1}\mathbf{e}^{(n)}$. From the LU factorization, $A^{-1}\mathbf{e}^{(n)} = U^{-1}L^{-1}\mathbf{e}^{(n)}$. Since L is lower triangular with unit diagonal, $L^{-1}\mathbf{e}^{(n)} = \mathbf{e}^{(n)}$, so $A^{-1}\mathbf{e}^{(n)} = U^{-1}\mathbf{e}^{(n)}$. Now, since U is upper-triangular, the last entry of $U^{-1}\mathbf{e}^{(n)}$ is $u_{n,n}^{-1}$. \square

LEMMA 2.4. *Let A be a tridiagonal and diagonally dominant $n \times n$ matrix with positive diagonal entries, and let $A = LU$ be its LU factorization with unit diagonal on L . Then $u_{i,i} \geq |u_{i,i+1}|$ for $1 \leq i \leq n-1$.*

Proof. First consider the LU factorization of A , as

$$A = \begin{bmatrix} 1 & & & & \\ \ell_{2,1} & 1 & & & \\ & \ell_{3,2} & 1 & & \\ & & \ddots & \ddots & \\ & & & \ell_{n,n-1} & 1 \end{bmatrix} \begin{bmatrix} u_{1,1} & u_{1,2} & & & \\ & u_{2,2} & u_{2,3} & & \\ & & u_{3,3} & u_{3,4} & \\ & & & \ddots & \ddots \\ & & & & u_{n,n} \end{bmatrix}.$$

From here, we can directly calculate that $u_{1,1} = a_{1,1}$, $u_{1,2} = a_{1,2}$ and, for $i > 1$,

$$\begin{aligned} u_{i,i+1} &= a_{i,i+1}, \\ \ell_{i,i-1} &= a_{i,i-1}/u_{i-1,i-1}, \\ u_{i,i} &= a_{i,i} - \ell_{i,i-1}u_{i-1,i} = a_{i,i} - a_{i,i-1} \frac{u_{i-1,i}}{u_{i-1,i-1}}. \end{aligned}$$

Now, consider a proof of the theorem by induction. For the base case, we have $u_{1,1} \geq |u_{1,2}|$ from the original assumption on diagonal dominance of A . For the inductive step, assume $u_{i-1,i-1} \geq |u_{i-1,i}|$. Then,

$$u_{i,i} \geq a_{i,i} - |a_{i,i-1}| \left| \frac{u_{i-1,i}}{u_{i-1,i-1}} \right| \geq a_{i,i} - |a_{i,i-1}| \geq |a_{i,i+1}|,$$

where the last step follows by diagonal dominance of A . Since $u_{i,i+1} = a_{i,i+1}$, this completes the inductive step and the proof. \square

COROLLARY 2.5. *Let A be the $N \times N$ discretization matrix of (1.1), as given in (2.3), partitioned as in (2.6). Then,*

$$(A_{IL}A_{LL}^{-1}A_{LI})_{1,1} \leq |a_{N_L+1,N_L}| = (A_{IL})_{1,N_L}.$$

Proof. From above, we have that

$$(A_{IL}A_{LL}^{-1}A_{LI})_{1,1} = a_{N_L+1,N_L}a_{N_L,N_L+1}(A_{LL}^{-1})_{N_L,N_L}.$$

Lemma 2.3 shows that if $A_{LL} = LU$ is the LU factorization of A_{LL} (with unit diagonal on L), then $(A_{LL}^{-1})_{N_L,N_L} = (u_{N_L,N_L})^{-1}$, and

$$(2.8) \quad (A_{IL}A_{LL}^{-1}A_{LI})_{1,1} = a_{N_L+1,N_L} \frac{a_{N_L,N_L+1}}{u_{N_L,N_L}}.$$

Extending the induction argument from Lemma 2.4, we have that

$$u_{N_L,N_L} = a_{N_L,N_L} - a_{N_L,N_L-1} \frac{u_{N_L-1,N_L}}{u_{N_L,N_L}} \geq a_{N_L,N_L} - |a_{N_L,N_L-1}|.$$

From the definition of the stencil in (2.3), this gives $u_{N_L,N_L} \geq |a_{N_L,N_L+1}|$. Using this to bound the right-hand side of (2.8) gives the stated result. \square

We are now ready to state and prove our main result, on the eigenvalues of the preconditioned system.

THEOREM 2.6. *Let A be the $N \times N$ tridiagonal matrix given by the stencil in (2.3), block partitioned as in (2.6) and let M be the preconditioner defined in (2.7). Assume that there is a constant, α , such that the discretization mesh satisfies $\alpha/N \leq h_i$ for $N_L + 1 \leq i \leq N$. Then, any eigenvalue, λ , of $M^{-1}A$ satisfies*

$$(2.9) \quad 1 - \frac{8\varepsilon N}{\underline{C}\alpha} \leq \lambda \leq 1,$$

where $\underline{C} > 0$ is defined in (2.1).

Proof. From Theorem 2.2, we have that all of the eigenvalues of $M^{-1}A$ are either 1 (and trivially satisfy the bound) or are eigenvalues of $S_M^{-1}S_A$. Note that we can write $S_A = S_M - \hat{L}$, where \hat{L} is a strictly lower-triangular matrix, so that

$$S_M^{-1}S_A = S_M^{-1}(S_M - \hat{L}) = I - S_M^{-1}\hat{L}.$$

Consequently, any eigenvalue, λ , of $S_M^{-1}S_A$ can be written as $\lambda = 1 - \gamma$, where γ is an eigenvalue of $S_M^{-1}\hat{L}$. Note, also, that this preserves algebraic and geometric multiplicities of the eigenvalues.

Now, we recognize $S_M^{-1}\hat{L}$ as the iteration matrix for a reverse-ordered Gauss-Seidel iteration on S_A , and that since S_A is tridiagonal, it is a 2-cyclic matrix. Thus, by classical arguments [25], we have that any eigenvalue, γ , of $S_M^{-1}\hat{L}$ is either zero or the square of an eigenvalue of the corresponding Jacobi iteration matrix. Here, we recognize that this relationship does *not* preserve geometric multiplicities, so that $\gamma = 0$ may correspond to an eigenvalue whose algebraic multiplicity may be larger than its geometric multiplicity. Writing D_A as the diagonal matrix whose entries match those of S_A , we can naturally write

$$I - D_A^{-1}S_A = \begin{bmatrix} 0 & b_1 & & & & \\ b_{-1} & 0 & b_2 & & & \\ & b_{-2} & 0 & b_3 & & \\ & & \ddots & \ddots & \ddots & \\ & & & b_{2-N_I} & 0 & b_{N_I-1} \\ & & & & b_{1-N_I} & 0 \end{bmatrix},$$

with natural definitions of b_k and b_{-k} for $1 \leq k \leq N_I - 1$, noting that S_A differs from A_{II} only in its first entry. We can define the diagonal scaling matrix Σ , by taking $\sigma_{1,1} = 1$, then defining $\sigma_{k+1,k+1} = \sqrt{b_k/b_{-k}}\sigma_{k,k}$ for $2 \leq k \leq N_I - 1$, noting that both b_k and b_{-k} are positive. By direct calculation, we then have the similarity transform

$$\Sigma(I - D_A^{-1}S_A)\Sigma^{-1} = \begin{bmatrix} 0 & \sqrt{b_{-1}b_1} & & & \\ \sqrt{b_{-1}b_1} & 0 & \sqrt{b_{-2}b_2} & & \\ & \sqrt{b_{-2}b_2} & 0 & \ddots & \\ & & \ddots & \ddots & \\ & & & 0 & \sqrt{b_{1-N_I}b_{N_I-1}} \\ & & & \sqrt{b_{1-N_I}b_{N_I-1}} & 0 \end{bmatrix}.$$

This is symmetric, so Geršgorin's Theorem implies that any eigenvalue, μ , of $I - D_A^{-1}S_A$ must be real and satisfy

$$|\mu| \leq 2 \max_{1 \leq k \leq N_I-1} \sqrt{b_{-k}b_k}.$$

Considering the stencil in (2.3), for $2 \leq k \leq N_I - 1$, we have

$$\begin{aligned} b_{-k} &= \frac{-a_{N_L+k+1, N_L+k}}{a_{N_L+k+1, N_L+k+1}} \\ &= \frac{\frac{\varepsilon}{\bar{h}_{N_L+k+1}h_{N_L+k+1}}}{\frac{\varepsilon}{\bar{h}_{N_L+k+1}} \left(\frac{1}{h_{N_L+k+1}} + \frac{1}{h_{N_L+k+2}} \right) + \frac{c_{N_L+k+1}}{h_{N_L+k+2}} + r_{N_L+k+1}} \leq \frac{2\varepsilon}{\underline{C}h_{N_L+k+1}} \leq \frac{2\varepsilon N}{\underline{C}\alpha}, \\ b_k &= \frac{-a_{N_L+k, N_L+k+1}}{a_{N_L+k, N_L+k}} \\ &= \frac{\frac{\varepsilon}{\bar{h}_{N_L+k}h_{N_L+k+1}} + \frac{c_{N_L+k}}{h_{N_L+k+1}}}{\frac{\varepsilon}{\bar{h}_{N_L+k}} \left(\frac{1}{h_{N_L+k}} + \frac{1}{h_{N_L+k+1}} \right) + \frac{c_{N_L+k}}{h_{N_L+k+1}} + r_{N_L+k}} \leq 1 \end{aligned}$$

The same bound is true for b_{-1} . For the remaining term, we use the bound in Corollary 2.5 to get

$$b_1 \leq \frac{\frac{\varepsilon}{\bar{h}_{N_L+1}h_{N_L+2}} + \frac{c_{N_L+1}}{h_{N_L+2}}}{\frac{\varepsilon}{\bar{h}_{N_L+1}} \left(\frac{1}{h_{N_L+1}} + \frac{1}{h_{N_L+2}} \right) + \frac{c_{N_L+1}}{h_{N_L+2}} + r_{N_L+1} - \frac{\varepsilon}{\bar{h}_{N_L+1}h_{N_L+1}}} \leq 1.$$

Taken together, these show that any eigenvalue, μ , of the Jacobi iteration matrix for S_A satisfies the bound that

$$|\mu| \leq 2\sqrt{\frac{2\varepsilon N}{\underline{C}\alpha}}.$$

Thus, the eigenvalues, γ , of $S_M^{-1}\hat{L}$ satisfy the bound

$$0 \leq \gamma \leq \frac{8\varepsilon N}{\underline{C}\alpha}.$$

Noting that the eigenvalues of $M^{-1}A$ are either 1 or $1 - \gamma$ for an eigenvalue of $S_M^{-1}\hat{L}$ completes the proof. \square

The sharpness of Theorem 2.6 is investigated further in Section 2.5.

Remark 2.7. We note that Theorem 2.6 makes no assumptions on the meshwidths in the layer region. In fact, the theorem applies equally well to a discretization on a uniform mesh (where it shows that appropriately ordered Gauss-Seidel yields an effective stationary iteration in the singularly perturbed limit). Additionally, the theorem covers both cases of piecewise uniform (Shishkin) or graded (e.g., Bakhvalov) meshes.

Remark 2.8. The lower bound in (2.9) is useful only when ε is sufficiently small, relative to N , specifically, when

$$(2.10) \quad \varepsilon N \leq C\alpha/8.$$

This is not a significant restriction; for larger ε , a uniform mesh is sufficient to resolve all aspects of the solution. Furthermore, as per the discussion in Section 2.1, if εN is so large that (2.10) does not hold, a discretization using central differences is stable on a uniform mesh, and specialized preconditioners are not needed.

2.5. Numerical Experiments. In this section, we verify the robustness of the bounds presented in Theorem 2.6, and then investigate the practical issue of determining a suitable stopping criterion when GMRES is preconditioned with M as given in (2.7).

Our test problem is

$$(2.11) \quad -\varepsilon u'' - (2 + \sin(5x))u' + u = 4e^{-x} \text{ on } (0, 1), \quad u(0) = u(1) = 0.$$

A computed solution when $\varepsilon = 10^{-2}$ is shown in Figure 2.2.

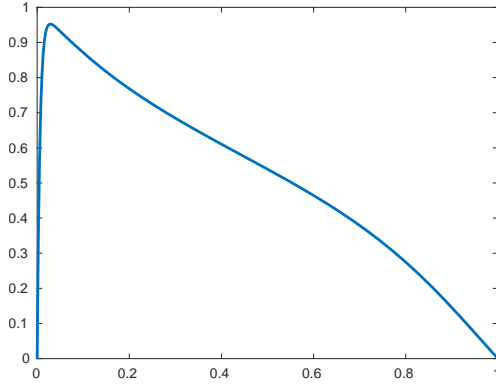


FIG. 2.2. Solution to (2.11) with $\varepsilon = 10^{-2}$

In Table 2.1, we verify that the error bounds reported in (2.5) are sharp: the upwind scheme applied on the Shishkin mesh of Section 2.2 yields a solution with error that is bounded independently of ε . We also show ρ^N , the estimated rate of convergence for the smallest value of ε . It is in agreement with (2.5): the error is proportional to $N^{-1} \ln N$.

Since an analytical solution to (2.11) is not available, for each N , these errors are estimated by comparing with a benchmark solution computed on a mesh with the same transition points, but $64N$ mesh intervals.

Our numerical experiments have verified that Theorem 2.6 is correct and quite sharp. For the data corresponding to the first column of Table 2.1, and denoting

TABLE 2.1
Error, in the discrete maximum norm, for (2.11).

ε	$N = 128$	$N = 256$	$N = 512$	$N = 1024$	$N = 2048$
1	2.425×10^{-3}	1.220×10^{-3}	6.120×10^{-4}	3.065×10^{-4}	1.534×10^{-4}
10^{-1}	2.725×10^{-2}	1.409×10^{-2}	7.173×10^{-3}	3.619×10^{-3}	1.818×10^{-3}
10^{-2}	4.963×10^{-2}	3.007×10^{-2}	1.742×10^{-2}	9.851×10^{-3}	5.473×10^{-3}
10^{-3}	4.822×10^{-2}	2.927×10^{-2}	1.699×10^{-2}	9.627×10^{-3}	5.357×10^{-3}
10^{-4}	4.800×10^{-2}	2.914×10^{-2}	1.692×10^{-2}	9.586×10^{-3}	5.334×10^{-3}
10^{-5}	4.798×10^{-2}	2.913×10^{-2}	1.691×10^{-2}	9.582×10^{-3}	5.332×10^{-3}
10^{-6}	4.798×10^{-2}	2.912×10^{-2}	1.691×10^{-2}	9.581×10^{-3}	5.332×10^{-3}
10^{-7}	4.798×10^{-2}	2.912×10^{-2}	1.691×10^{-2}	9.581×10^{-3}	5.332×10^{-3}
10^{-8}	4.798×10^{-2}	2.912×10^{-2}	1.691×10^{-2}	9.581×10^{-3}	5.332×10^{-3}
ρ^N	0.678	0.720	0.784	0.820	0.846

(a numerical estimate for) the smallest eigenvalue of $M^{-1}A$ as λ_{\min} , we verify that $\lambda_{\min} \geq 1 - 8\varepsilon N/(\underline{C}\alpha)$ by plotting $1 - \lambda_{\min}$ and $8\varepsilon N/(\underline{C}\alpha)$, where the largest valid value of α is taken. Indeed, for the range of N and ε reported in Table 2.1, we observe that λ_{\min} is found between $1 - 4\varepsilon N/(\underline{C}\alpha)$ and $1 - \varepsilon N/(2\underline{C}\alpha)$, as long as (2.10) holds.

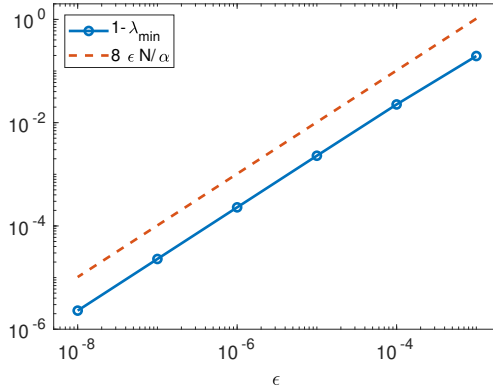


FIG. 2.3. Comparison of $1 - \lambda_{\min}$ and $8\varepsilon N/(\underline{C}\alpha)$, where λ_{\min} is the smallest eigenvalue of $M^{-1}A$, for $N = 128$, and $\varepsilon = 10^{-3}, 10^{-4}, \dots, 10^{-8}$.

2.5.1. Stopping criterion. Let U^E be the exact solution to the linear system arising from the scheme of Section 2.1, and $U^{(k)}$ be the k th iterate computed by an iterative solver. Let $g(N)$ be the expected discretization error; for example, for the mesh and method we consider here,

$$g(N) := \|u - U^E\|_{\infty} \leq CN^{-1} \ln N.$$

(See, e.g., [20], for analysis of a mesh where fully first-order convergence is expected.) We wish to iterate until

$$\|u - U^{(k)}\|_{\infty} \leq \|u - U^E\|_{\infty} + \|U^E - U^{(k)}\|_{\infty} \leq Cg(N)$$

where C is a moderate constant. Of course, we cannot compute $E^{(k)} = U^E - U^{(k)}$, but we can compute the residual $R^{(k)} = F - AU^{(k)} = AE^{(k)}$. Therefore we write

$E^{(k)} = A^{-1}R^{(k)}$, giving

$$\|U^E - U^{(k)}\|_\infty \leq \|A^{-1}\|_\infty \|R^{(k)}\|_\infty.$$

In contrast to the stopping criterion proposed in [13] for reaction-diffusion problems, in which $\|A^{-1}\|_\infty$ is unbounded when $\varepsilon \rightarrow 0$, for convection-diffusion problems, the system matrix A defined in (2.6) is an M-matrix. Thus, it is easy to verify that (see, for example, [19])

$$\|A^{-1}\|_\infty \leq C.$$

Therefore, we iterate until $\|R^{(k)}\|_\infty \leq Kg(N)$, for some user-chosen parameter K . Numerical experience suggests that taking $K = \|U^E\|_\infty$ is reasonable (i.e., an $\mathcal{O}(1)$ value).

2.5.2. Performance of the preconditioner. The discretization of (2.11) leads to a tridiagonal system which is easily solved using direct methods, even for very large values of the discretization parameter, N . However, it is instructive to consider the performance of an iterative solver for this problem, when preconditioned with M as defined in (2.7).

To that end, in Table 2.2, we report the number of iterations required by the MATLAB `gmres` function [26], modified slightly to implement the stopping criterion, and with no restarts. The results are for those values of ε and N included in Table 2.1 for which (2.10) holds. They show that, as expected, few iterations are required as $\varepsilon \rightarrow 0$. The greatest number of iterations are required for largest reported values of ε and N , where, although (2.10) holds, one has that $\varepsilon N > \underline{C}\alpha/2$. In all other cases, $\varepsilon N \ll \underline{C}\alpha$, and few iterations are required to ensure convergence. For example, if $\varepsilon N \leq 0.01$, then no more than 4 iterations are required in any case.

TABLE 2.2
Iteration counts for GMRES preconditioned with M in (2.7)

ε	$N = 128$	$N = 256$	$N = 512$	$N = 1024$	$N = 2048$
10^{-3}	4	—	—	—	—
10^{-4}	2	4	6	14	38
10^{-5}	1	2	3	5	9
10^{-6}	1	1	2	2	4
10^{-7}	1	1	1	2	2
10^{-8}	1	1	1	1	2

3. Two-dimensional problems. We now consider the two-dimensional problem on the unit square given in (1.2), with homogeneous Dirichlet boundary conditions on all four sides and $r(x, y) \geq 0$. We focus on two cases, both where $c(x, y)$ is componentwise non-negative. In the first case, we fix $c_2(x, y) = 0$ and require $c_1(x, y) > 0$. From the standard theory of convection-diffusion problems, solutions to (1.2) in this case are expected to exhibit parabolic (characteristic) boundary layers of width $\mathcal{O}(\sqrt{\varepsilon} \ln(1/\varepsilon))$ along $y = 0$ and $y = 1$, and a single exponential boundary layer of width $\mathcal{O}(\varepsilon \ln(1/\varepsilon))$ along $x = 0$. We will focus our discussion on the case where the forcing function is *compatible* with the boundary conditions, so that no layer forms along $y = 1$, noting that this is solely for convenience and that all constructions could be directly extended to handle the case of two parabolic layers. The second case that we consider is when both $c_1(x, y) > 0$ and $c_2(x, y) > 0$, which leads to the formation of two exponential layers in the solution, along $x = 0$ and $y = 0$.

For both problems, we make use of tensor-product Shishkin meshes for the discretization, now defining separate transition points in the x - and y -directions, denoted by τ_x and τ_y , respectively. A sketch of such a mesh for the case with one parabolic and one exponential layer is shown in Figure 3.1. We make the following standard choices for the transition points on an $N \times N$ mesh for the first case, where we assume $0 < \underline{C} < c_1(x, y)$ for all $(x, y) \in (0, 1)^2$,

$$(3.1) \quad \tau_x = \min \left\{ \frac{1}{2}, \frac{\sigma \varepsilon}{\underline{C}} \ln(N) \right\}, \quad \text{and} \quad \tau_y = \min \left\{ \frac{1}{2}, \sigma \sqrt{\varepsilon} \ln(N) \right\}.$$

Here, we take $\sigma = 5/2$ as a value that is at least as large as the order of the discretization scheme discussed below. For the case of two exponential layers, we assume that both $0 < \underline{C}_1 < c_1(x, y)$ and $0 < \underline{C}_2 < c_2(x, y)$, and take

$$(3.2) \quad \tau_x = \min \left\{ \frac{1}{2}, \frac{\sigma \varepsilon}{\underline{C}_1} \ln(N) \right\} \quad \text{and} \quad \tau_y = \min \left\{ \frac{1}{2}, \frac{\sigma \varepsilon}{\underline{C}_2} \ln(N) \right\}.$$

In both cases, we then form a standard tensor-product Shishkin mesh, by first dividing the unit interval on the x -axis into $N/2$ equal-sized intervals from 0 to τ_x and $N/2$ equal-sized intervals from τ_x to 1 to form the mesh Ω_x^N , then dividing the unit interval on the y -axis into $N/2$ equal-sized intervals from 0 to τ_y and $N/2$ equal-sized intervals from τ_y to 1 to form the mesh Ω_y^N and, finally, forming the standard (quadrilateral) tensor-product mesh, $\Omega_x^N \times \Omega_y^N$. While we focus on the Shishkin case below, we note that the ideas developed could equally-well be applied to many fitted tensor-product mesh constructions appropriate for such singularly perturbed problems; the key idea that is required for what follows is the ability to identify a transition point between the “interior” region of the mesh, where meshwidths are bounded below by an $\mathcal{O}(1/N)$ value, and the layer regions, where meshwidths may be much smaller.

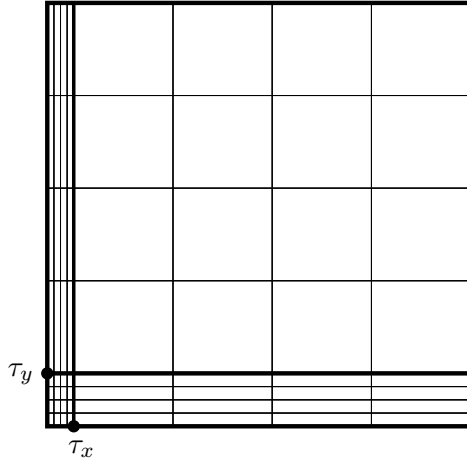


FIG. 3.1. Sketch of a tensor-product Shishkin mesh for the case of a parabolic layer along the edge $y = 0$ and an exponential layer along the edge $x = 0$.

On such a mesh, we make use of a standard upwind finite-difference discretization for (1.2) on a non-uniform mesh. At a mesh point (x_i, y_j) for $1 \leq i, j \leq N$, we

define $h_i = x_i - x_{i-1}$ and $k_j = y_j - y_{j-1}$, with h_{i+1} and k_{j+1} defined similarly, and $\bar{h}_i = (h_i + h_{i+1})/2$ and $\bar{k}_j = (k_j + k_{j+1})/2$. The discretization then takes the same pattern as a standard 5-point finite-difference operator, with values

$$\begin{pmatrix} \frac{-\varepsilon}{\bar{h}_i \bar{h}_i} & \frac{\varepsilon}{\bar{h}_i} \left(\frac{1}{h_i} + \frac{1}{h_{i+1}} \right) + \frac{\varepsilon}{\bar{k}_j} \left(\frac{1}{k_j} + \frac{1}{k_{j+1}} \right) + \frac{c_{1,ij}}{h_{i+1}} + \frac{c_{2,ij}}{k_{j+1}} + r_{ij} & \frac{-\varepsilon}{\bar{h}_i \bar{h}_{i+1}} - \frac{c_{1,ij}}{\bar{h}_{i+1}} \\ \frac{-\varepsilon}{\bar{k}_j \bar{k}_j} \end{pmatrix},$$

where $c_{1,ij} = c_1(x_i, y_j)$, $c_{2,ij} = c_2(x_i, y_j)$, and $r_{ij} = r(x_i, y_j)$. We note that the upwind finite-difference discretization results in a discretization matrix that is both irreducibly diagonally dominant and an M-matrix, since we have $c_{1,ij} > 0$, $c_{2,ij} \geq 0$, and $r_{ij} \geq 0$.

3.1. Preconditioner construction. In order to develop the preconditioner, we consider reordering and partitioning the discretization matrix, A , into block four-by-four structure, writing

$$A = \begin{bmatrix} A_{CC} & A_{CX} & A_{CY} & A_{CI} \\ A_{XC} & A_{XX} & A_{XY} & A_{XI} \\ A_{YC} & A_{YX} & A_{YY} & A_{YI} \\ A_{IC} & A_{IX} & A_{IY} & A_{II} \end{bmatrix},$$

where we use the subscripts C to denote the corner region, i.e., the mesh points in the rectangle $[0, \tau_x] \times [0, \tau_y]$, Y to denote the region $(\tau_x, 1] \times [0, \tau_y]$, X to denote the region $[0, \tau_x] \times (\tau_y, 1]$, and I to denote the interior region, i.e., $(\tau_x, 1] \times (\tau_y, 1]$. As above, we include the transition points in the edge and corner regions, with the corner region including points with both $x_i = \tau_x$ and $y_j = \tau_y$, while the edge regions include just the transition points adjacent to the interior region. For simplicity in explanation, we assume that grid points in each block are ordered lexicographically by index in the mesh, from their lower-left corners to their upper-right corners.

In both cases under consideration, we have a convective term in our PDE that “pushes” information from right-to-left and, in the case of two exponential layers, from top-to-bottom. Ordering the discretization as above, a natural structure for a preconditioner, then, is as a block upper-triangular matrix,

$$(3.3) \quad M = \begin{bmatrix} M_{CC} & A_{CX} & A_{CY} & A_{CI} \\ 0 & M_{XX} & A_{XY} & A_{XI} \\ 0 & 0 & M_{YY} & A_{YI} \\ 0 & 0 & 0 & M_{II} \end{bmatrix},$$

since solution of $Mz = r$ then propagates information from the interior region to all three other regions, while information from the two edge regions is propagated to the corner region, matching the natural convective structure of the system. Since the off-diagonal blocks of the matrix are only needed for matrix-vector products to propagate information from solves with the diagonal blocks, there is no computational advantage to approximating these. In contrast, we consider in detail how to best approximate each of the diagonal blocks so that the overall cost of solving the linear system $Mz = r$ is only $\mathcal{O}(N^2)$, matching the asymptotic cost of a matrix-vector multiplication with the system matrix, A .

We treat the four diagonal blocks of M in (3.3) separately, as follows.

- M_{II} : This block is associated with points in the interior region $(\tau_x, 1] \times (\tau_y, 1]$. Around a mesh point in this region, we have $h_i, h_{i+1} \geq C/N$ as well as $k_j, k_{j+1} \geq C/N$, thus, the diffusion terms in the stencil are of size $\mathcal{O}(\varepsilon N^2)$ while the convection terms are $\mathcal{O}(N)$ in size. Under the typical assumption that $\varepsilon N \ll 1$, this says that the convection term(s) dominate, and that a good approximation of A_{II} is by its upper-triangular part, resulting in a downstream Gauss-Seidel approximation that sweeps from the upper-right corner of the interior region to the bottom-left corner. In the case where there is a parabolic layer, the structure is even simpler, since $c_{2,ij} = 0$ and the system is dominated by only its diagonal and one off-diagonal term. Here, any Gauss-Seidel ordering that sweeps from right-to-left would be acceptable, but it is simpler to use the same ordering in both cases. We note the cost of a solve with M_{II} is bounded by that of a matrix-vector multiplication with A_{II} , achieving our cost goal.
- M_{YY} : This block is associated with points in the region $(\tau_x, 1] \times [0, \tau_y]$. At a mesh point here we have $h_i, h_{i+1} \geq C/N$, while we have much smaller values for k_j and k_{j+1} . In the case of a classical Shishkin mesh for a parabolic boundary layer in this region, for example, we have $k_j = k_{j+1} \approx 2\sqrt{\varepsilon} \ln(N)/N$, while for a classical Shishkin mesh for an exponential boundary layer in this region (when $c_{2,ij} \neq 0$), we have $k_j = k_{j+1} \approx 2\varepsilon \ln(N)/N$. In the case of a parabolic layer, only one off-diagonal term (that to the “West”, from (x_i, y_j) to (x_{i-1}, y_{j-1})) is asymptotically smaller than the rest, with the meshwidth in the y -direction leading to off-diagonal entries of size $\mathcal{O}(N^2/\ln^2(N))$ in the “North” and “South” directions, while the convection term leads to the “East” off-diagonal entry having size $\mathcal{O}(N)$. In order to account for these three terms, we approximate A_{YY}^{-1} by a block downstream Gauss-Seidel approximation, where we use line-solves along lines of constant x -coordinate, ordered from right-to-left. These line solves are implemented using Thomas’ algorithm, which gives $\mathcal{O}(N)$ cost to each solve and an $\mathcal{O}(N^2)$ cost to the inversion of M_{YY} constructed in this way. For the case of two exponential layers, the diffusion terms in the y -direction become dominant, of size $\mathcal{O}(N^2/(\varepsilon \ln^2(N)))$, again prompting the use of line solves along lines of constant x -coordinate to approximate A_{YY}^{-1} . While the ordering is less important here, we keep the right-to-left ordering for simplicity.
- M_{XX} : this block is associated with points in the region $[0, \tau_x] \times (\tau_y, 1]$. In contrast to the mesh points in the region associated with M_{YY} , here we have $k_j, k_{j+1} \geq C/N$, while we have much smaller values for h_i and h_{i+1} in order to resolve the exponential boundary layer in the solution at $x = 0$. On a classical Shishkin mesh, for example, we expect $h_i = h_{i+1} \approx 2\varepsilon \ln(N)/N$. This results in relatively small contributions to the matrix from the diffusion terms in the y -direction, which are of size $\mathcal{O}(\varepsilon N^2)$. In comparison, the diffusion terms in the x -direction are of size $\mathcal{O}(N^2/(\varepsilon \ln^2(N)))$, while the convection terms in the x -direction are of size $\mathcal{O}(N/(\varepsilon \ln(N)))$. This motivates approximating A_{XX}^{-1} using line solves along lines of constant y -coordinate. While the North coefficient is never large, the case of two exponential layers gives a y -direction convection contribution of size $\mathcal{O}(N)$; thus, we perform these line solves sequentially, sweeping from the top of the mesh downwards, to resolve the convection in the downward direction. As in the Y region, the cost of each line solve is $\mathcal{O}(N)$ operations, and we perform $\mathcal{O}(N)$ of them, giving a total cost of inverting M_{XX} that is still $\mathcal{O}(N^2)$.

We devote Section 3.2 to the approximation in the corner region of the mesh, but first pause to consider a simple bound on the convergence rate of an idealized form of the preconditioner. Using the approximations above, we can define

$$\hat{M} = \begin{bmatrix} A_{CC} & A_{CX} & A_{CY} & A_{CI} \\ 0 & M_{XX} & A_{XY} & A_{XI} \\ 0 & 0 & M_{YY} & A_{YI} \\ 0 & 0 & 0 & M_{II} \end{bmatrix},$$

and consider the classical theory of regular splittings [25, §3.6]. Since A is an irreducibly diagonally dominant M-matrix, the splitting of $A = \hat{M} - \hat{N}$ is a regular splitting (since \hat{M} inherits the property of being an M-matrix by its construction from A [25, Theorem 3.25], and the implicit definition of $\hat{N} = \hat{M} - A$ yields a component-wise non-negative matrix). Thus, [25, Theorem 3.29] gives us a bound on the spectral radius of the stationary iteration whose error-propagation operator is given by $I - \hat{M}^{-1}A$, as

$$\rho(I - \hat{M}^{-1}A) = \frac{\rho(A^{-1}\hat{N})}{1 + \rho(A^{-1}\hat{N})} < 1.$$

We note that the quotient given is monotone increasing with $\rho(A^{-1}\hat{N})$, so that any upper bound that we get on this spectral radius gives an upper bound on that of $I - \hat{M}^{-1}A$,

$$\rho(A^{-1}\hat{N}) \leq K \Rightarrow \rho(I - \hat{M}^{-1}A) \leq \frac{K}{1 + K}.$$

A natural bound to use is that

$$\rho(A^{-1}\hat{N}) \leq \|A^{-1}\hat{N}\| \leq \|A^{-1}\| \|\hat{N}\|,$$

where we will consider the standard matrix norm induced by the discrete maximum norm. By a standard barrier-function technique [21], there exists a constant, C , such that $\|A^{-1}\| \leq C$ (taking the vector, W , whose value at the degree of freedom associated with grid point (x_i, y_j) is $1 + x_i$, so that $AW \geq \underline{C}$ (or \underline{C}_x) in the pointwise sense, but $\|W\| \leq 2$). For the bound on $\|\hat{N}\|$, we note that \hat{N} has at most two nonzero entries in each of its rows or columns (by construction), and that all of these entries are of the form of either $\varepsilon/(\bar{h}_i h_i)$ or $\varepsilon/(\bar{k}_j k_j)$. All of the entries in \hat{N} , however, are associated with points (x_i, y_j) where there exists a constant, C , such that $h_i, \bar{h}_i, k_j, \bar{k}_j \geq C/N$ for all such entries dropped from A . Thus, there exists a constant, C , such that $\|\hat{N}\| < C\varepsilon N^2$. Taken together, these give us the bound that

$$\rho(I - \hat{M}^{-1}A) \leq \frac{C\varepsilon N^2}{1 + C\varepsilon N^2}.$$

We note that this bound is suboptimal in comparison to Theorem 2.6, since we typically assume that $\varepsilon N \ll 1$, but not that εN^2 is bounded by a constant. Nonetheless, it is an improvement on standard bounds on the condition number of the unpreconditioned system, $\kappa(A) \leq C \frac{N^2}{\varepsilon(\ln N)^2}$, or a diagonally preconditioned system, $\kappa(\hat{D}^{-1}A) \leq C \frac{N^2}{\ln N}$ [21]. As always with nonsymmetric systems, convergence of either a stationary or Krylov iteration depends on much more than the condition number of the system; however, this is an indication that the preconditioner construction should lead to improved performance for iterations preconditioned in this way.

3.2. Multigrid for the corner region. Finally, we consider the case of the approximation of A_{CC} , corresponding to mesh points in $[0, \tau_x] \times [0, \tau_y]$. In this region, the mesh is refined in both the x - and y -directions, leading to discrete problems where the diffusion terms in both directions are no longer dominated by the convection terms. In such cases, multigrid methods are well-recognized as providing excellent approximations to A_{CC}^{-1} that can be implemented with $\mathcal{O}(N^2)$ computational cost. Here, we discuss the details of the construction of such methods. Since the methods we adopt are quite different for the two cases we consider, we present the methods independently.

On a classical Shishkin mesh for a problem with one parabolic and one exponential boundary layer, the transition points are as in (3.1), and we expect $h_i = h_{i+1} \approx 2\varepsilon \ln(N)/N$ and $k_j = k_{j+1} \approx 2\sqrt{\varepsilon} \ln(N)/N$. This gives off-diagonal entries of size $\mathcal{O}(N^2/\ln^2(N))$ in the North and South directions on the mesh, but of size $\mathcal{O}(N^2/(\varepsilon \ln^2(N)))$ in the West and East directions. In essence, the problem much more resembles a classical anisotropic diffusion operator than a singularly perturbed convection-diffusion operator. As a result, we approximate A_{CC}^{-1} by the action of a multigrid cycle appropriate to an anisotropic problem. In particular, we make use of a semi-coarsening multigrid algorithm in this case, where the coarse grids are formed by factor-2 coarsening in only the x -direction. As a relaxation scheme, we use pointwise Gauss-Seidel, again ordered in a “downstream” direction, ordered from the top right point in the corner region to the bottom left. We use a standard V(1,1) cycling strategy, and approximate a solve on the coarsest grid by four sweeps of the downstream Gauss-Seidel relaxation.

In order to properly account for possible variations in the mesh size and the effects of the convection term, we use a Galerkin coarsening algorithm, with each coarse-grid operator formed by the triple-product of a restriction operator, the fine-grid operator, and an interpolation operator. For ease of construction, on the finest grid (the discretization mesh), we perform a row-wise rescaling of the finite-difference discretization (only within the multigrid cycle on the corner region, with a corresponding rescaling on the residual in this region before the cycle is applied), multiplying the row of the matrix that corresponds to node (x_i, y_j) by $\bar{h}_i \bar{k}_j$; in essence, this rescales the problem from a finite-difference-like scaling to one more akin to a finite-element discretization, where Galerkin coarsening is more natural. With this rescaling, we define a one-dimensional interpolation operator from the coarse grid to fine-grid node (x_i, y_j) by first “collapsing” the matrix stencil corresponding to this row in the North-South direction into a 3-point operator. Adopting the notation of writing $a_{(i,j),(k,\ell)}$ for the entry in the matrix in row corresponding to node (x_i, y_j) and column corresponding to node (x_k, y_ℓ) , we define the interpolation operator to fine-grid node (x_i, y_j) with entries

$$\begin{aligned} & - \frac{a_{(i,j),(i-1,j-1)} + a_{(i,j),(i-1,j)} + a_{(i,j),(i-1,j+1)}}{a_{(i,j),(i,j-1)} + a_{(i,j),(i,j)} + a_{(i,j),(i,j+1)}} \\ \text{and } & - \frac{a_{(i,j),(i+1,j-1)} + a_{(i,j),(i+1,j)} + a_{(i,j),(i+1,j+1)}}{a_{(i,j),(i,j-1)} + a_{(i,j),(i,j)} + a_{(i,j),(i,j+1)}}, \end{aligned}$$

for the weights of interpolation to fine-grid node (x_i, y_j) from the coarse-grid nodes associated with points (x_{i-1}, y_j) and (x_{i+1}, y_j) , respectively. Note that, while we have only a five-point stencil on the finest grid, the use of such Galerkin coarsening leads to nine-point stencils on all coarse grids, so we define the interpolation operator for the general case, and use a similar formula (adapted only to account for the coarsening)

on all grids. On all grids, we use the transpose of this operator as the restriction operator. Such an operator-induced interpolation operator is inspired by the BoxMG algorithm [2, 6], which uses a similar technique for anisotropic problems.

In preliminary numerical experiments, we found that using a single cycle of the above scheme did not lead to scalable results for a reasonable range of values for N and ε . Instead, we use a residual-reduction based tolerance, with M_{CC}^{-1} defined by performing as many cycles of the above method as needed to reduce the residual over the corner region of the mesh by a relative factor of 10^2 . In results reported below, this requires only 3 V-cycles; however, in other experiments, one or two more cycles were sometimes needed to reach this tolerance. Other options for gaining more robustness would be to increase the number of relaxation sweeps used on each level, or to switch to using a direct solver for the coarsest-grid system, but neither of these were thoroughly explored, as the strategy above did not lead to any apparent outliers in the data.

For the case of two exponential layers the transition points are of the same order of magnitude, see (3.2), and so the off-diagonal terms in A_{CC} are much more balanced in the x - and y -directions, allowing a simpler cycling structure. Here, we use a full-coarsening multigrid algorithm, coarsening by a factor of two in each direction. We use rediscritization to define the coarse-grid operators, and define geometric (bilinear) interpolation that accounts for the mesh spacing within the corner region. On Shishkin meshes, this coincides with the classical bilinear interpolation operator on uniform meshes, with interpolation weights of $1/2$ for fine-grid points that are directly adjacent to two coarse-grid points, and weights of $1/4$ for fine-grid points that are the centre of a coarse-grid cell. We again rescale by factors of $\bar{h}_i \bar{k}_j$ from the finite-difference to finite-element style of scaling, allowing us to use the transpose of this interpolation operator as restriction. (We note that such rescaling can be avoided on uniform meshes if one uses “full weighting” restriction, but this is equivalent to what we do.) The cycling structure in this case matches that for the case of one parabolic and one exponential layer, with the same approximate coarse-grid solve. Here, we found better results by defining M_{CC}^{-1} to correspond to stationary iteration with this cycle as needed to reduce the residual over the corner region of the mesh by a relative factor of 10^3 , which is again quickly reached (in 5 iterations for the results reported below).

We note that the approaches described above both differ significantly from the method of [9]. That paper described a multigrid algorithm to be applied to the same discretization on Shishkin meshes, but aimed at preconditioning the full system, and not just the discretization in the corner region. There, full-coarsening multigrid was applied using rediscritized coarse-grid operators and tuned intergrid transfer operators that were derived from the Shishkin mesh structure and the problem under consideration (with two exponential layers). Furthermore, an alternating line Gauss-Seidel relaxation was used. While the method proposed in [9] was generally successful, our overall preconditioner has a lower cost per cycle, because it focuses the numerical effort on the region of the mesh where it is needed most.

3.3. Numerical examples. We test the preconditioner developed above to solve two model problems, one that exhibits both a parabolic and an exponential layer, and one that exhibits two exponential layers. In both cases, we use the preconditioner described above with FGMRES [23] as the outer Krylov method. As in one dimension (and as discussed above), we have the bound that $\|A^{-1}\| < C$, for some constant C that is independent of ε and N , so we use a direct residual-based stopping tolerance on the expected almost-first-order discretization error on the Shishkin

meshes considered here, iterating until $\|R^{(k)}\| \leq 10N^{-1}\ln(N)$. While the above bound is on the discrete maximum norm of the matrix, the nature of FGMRES requires the stopping tolerance to be evaluated in the Euclidean norm, which we do. The algorithm is implemented in C and was compiled using gcc (version 8.2.0). All numerical results in this section were run, in serial, on a single core of a 2.4 GHz Xeon processor on a system with 192 GiB of RAM. For comparison, we consider a direct solution of the same linear systems using UMFPACK [5].

As a first example, for the case of one parabolic layer and one exponential layer, we consider the solution of

$$-\varepsilon\Delta u - u_x + u = f \text{ on } (0,1)^2,$$

with $f(x, y)$ chosen to yield a manufactured solution of

$$(3.4) \quad u(x, y) = \left(\cos\left(\frac{\pi x}{2}\right) - \frac{e^{-x/\varepsilon} - e^{-1/\varepsilon}}{1 - e^{-1/\varepsilon}} \right) \left(\frac{1 - e^{-y/\sqrt{\varepsilon}}}{1 - e^{-1/\sqrt{\varepsilon}}} - y^{5/2} \right).$$

To validate both the discretization and the chosen stopping tolerance, Table 3.1 shows discretization errors for the discrete solutions found by the algorithm. We note that these show the expected steadiness as $\varepsilon \rightarrow 0$, and the expected decay with large N . Preconditioned FGMRES iteration counts are shown in parentheses in Table 3.2. Here, we see that the iteration counts are quite steady as $\varepsilon \rightarrow 0$ and for varying values of N , aside from in the top-right corner of the table. Here, εN is not small enough for our heuristics to suggest that we are in the right range for the preconditioner to be effective, so the degradation in performance is not too surprising.

TABLE 3.1

Approximation error, measured in the discrete maximum norm, for manufactured solution in (3.4) generated by preconditioned FGMRES.

ε	$N = 2^7$	$N = 2^8$	$N = 2^9$	$N = 2^{10}$	$N = 2^{11}$
10^{-5}	3.822×10^{-2}	2.204×10^{-2}	1.242×10^{-2}	6.915×10^{-3}	3.783×10^{-3}
10^{-6}	3.823×10^{-2}	2.205×10^{-2}	1.244×10^{-2}	6.903×10^{-3}	3.783×10^{-3}
10^{-7}	3.823×10^{-2}	2.205×10^{-2}	1.244×10^{-2}	6.902×10^{-3}	3.783×10^{-3}
10^{-8}	3.823×10^{-2}	2.205×10^{-2}	1.244×10^{-2}	6.902×10^{-3}	3.783×10^{-3}

TABLE 3.2

CPU times (in seconds) for preconditioned FGMRES to achieve residual stopping tolerance for manufactured solution in (3.4). Corresponding iteration counts are given in parentheses.

ε	$N = 2^7$	$N = 2^8$	$N = 2^9$	$N = 2^{10}$	$N = 2^{11}$
10^{-5}	0.007 (3)	0.037 (4)	0.205 (5)	1.536 (9)	14.804 (23)
10^{-6}	0.007 (3)	0.028 (3)	0.165 (4)	0.868 (5)	4.581 (8)
10^{-7}	0.007 (3)	0.036 (4)	0.165 (4)	0.707 (4)	3.525 (5)
10^{-8}	0.009 (4)	0.036 (4)	0.165 (4)	0.868 (5)	3.524 (5)

The timing data presented in Table 3.2 shows that the CPU times scale largely as expected, growing proportionately to iteration counts and problem sizes. We note that for $\varepsilon < 10^{-5}$, the solution time for each problem on the 1024×1024 mesh is less than 1 second. This includes both the setup of the preconditioners (assembling the tridiagonal systems for the two edge-layer regions, performing the forward sweep of the

Thomas algorithm to factor these systems, and computing all necessary components on all levels of the multigrid algorithm for the corner region) and the preconditioned FGMRES solve time (including the residual and preconditioned residual calculations, modified Gram-Schmidt and Arnoldi steps, and construction of the solution once converged). As a comparison, Table 3.3 shows the speedup factors achieved for the preconditioned FGMRES iteration over a direct solution using UMFPACK on the same machine. As expected, the direct solution cost grows faster than $\mathcal{O}(N^2)$ as the mesh is refined and, so, the speedup generally increases with larger N (aside from the top-right corner, where iteration counts increase for the preconditioned FGMRES iteration). Table 3.3 also shows the *number of digits of accuracy* in the preconditioned FGMRES solution, defined as $\log_{10} (\|U^E\|_\infty / \|U^E - U^{(k)}\|_\infty)$, where U^E is the solution returned by UMFPACK (treated as the exact solution to the linear system) and $U^{(k)}$ is the iterative solution at iteration k , when the stopping tolerance is satisfied (as reported in Table 3.2). We note that for $\varepsilon < 10^{-5}$, we consistently match the direct solution to at least 3 digits of accuracy, and often more.

TABLE 3.3

Speedup of preconditioned FGMRES to achieve residual stopping tolerance for manufactured solution in (3.4) over direct solution using UMFPACK. In parentheses, the number of digits of accuracy in the preconditioned FGMRES solution.

ε	$N = 2^7$	$N = 2^8$	$N = 2^9$	$N = 2^{10}$	$N = 2^{11}$
10^{-5}	11.32 (4.0)	16.66 (3.6)	26.73 (2.1)	23.58 (1.7)	17.00 (2.6)
10^{-6}	13.28 (5.7)	22.66 (4.3)	29.35 (4.4)	34.82 (3.4)	43.68 (3.1)
10^{-7}	13.80 (4.1)	17.96 (5.7)	29.42 (5.0)	39.16 (4.5)	47.29 (5.1)
10^{-8}	10.79 (5.9)	16.82 (4.6)	25.32 (4.1)	27.38 (4.3)	40.68 (5.2)

Our second example is for the case of two exponential layers, where we solve

$$-\varepsilon \Delta u - 2u_x - 3u_y + u = f \text{ on } (0, 1)^2,$$

with $f(x, y)$ chosen to yield a manufactured solution of

$$(3.5) \quad u(x, y) = \left(\cos\left(\frac{\pi x}{2}\right) \right) \left(1 - e^{-2x/\varepsilon} \right) (1 - y)^3 \left(1 - e^{-3y/\varepsilon} \right)$$

Again, to validate both the discretization and the chosen stopping tolerance, Table 3.4 presents discretization errors for the solutions found by the algorithm, for a slightly different range of values of ε because of the different layer structure in this case. As before, this shows performance that is clearly bounded independently of ε and decays in the expected way with increasing N . Preconditioned FGMRES iterations are shown in parentheses in Table 3.5, and are very similar to those seen for the case of one parabolic and one exponential layer. As before, we note the degradation in performance in the upper-right corner of the table, for larger values of εN where the heuristics motivated above do not apply.

Considering the solution times shown in Table 3.5, we again see scaling as expected, with total time-to-solution that scales directly with iteration counts and problem sizes. Notably, the $\mathcal{O}(N^2)$ cost per iteration clearly scales through the largest problem size, and loss of scalability in solve times for large N is directly due to increasing iteration counts in the case where εN is large. As before, the reported timings include all costs for the setup and preconditioned FGMRES iterations, and we note that the cost per iteration is quite comparable for the preconditioner in this case to

TABLE 3.4

Approximation error, measured in the discrete maximum norm, for manufactured solution in (3.5) generated by preconditioned FGMRES.

ε	$N = 2^7$	$N = 2^8$	$N = 2^9$	$N = 2^{10}$	$N = 2^{11}$
10^{-4}	3.728×10^{-2}	2.260×10^{-2}	1.323×10^{-2}	7.570×10^{-3}	4.248×10^{-3}
10^{-5}	3.729×10^{-2}	2.261×10^{-2}	1.325×10^{-2}	7.572×10^{-3}	4.248×10^{-3}
10^{-6}	3.729×10^{-2}	2.261×10^{-2}	1.325×10^{-2}	7.572×10^{-3}	4.248×10^{-3}
10^{-7}	3.730×10^{-2}	2.261×10^{-2}	1.325×10^{-2}	7.572×10^{-3}	4.248×10^{-3}

TABLE 3.5

CPU times (in seconds) for preconditioned FGMRES to achieve residual stopping tolerance for manufactured solution in (3.5). Corresponding iteration counts are given in parentheses.

ε	$N = 2^7$	$N = 2^8$	$N = 2^9$	$N = 2^{10}$	$N = 2^{11}$
10^{-4}	0.010 (3)	0.041 (4)	0.266 (6)	2.656 (14)	37.690 (40)
10^{-5}	0.010 (4)	0.041 (4)	0.178 (4)	1.103 (6)	7.625 (10)
10^{-6}	0.010 (4)	0.041 (4)	0.221 (5)	0.921 (5)	3.771 (5)
10^{-7}	0.010 (4)	0.051 (5)	0.221 (5)	0.923 (5)	4.519 (6)

that of one parabolic and one exponential layer. Again, we see substantial speedups over a direct solve using UMFPACK, documented in Table 3.6, contrasting the poor scaling in N of a direct solver with the $\mathcal{O}(N^2)$ total solution cost seen here for smaller values of ε . Table 3.6 also shows the number of digits of accuracy in the preconditioned FGMRES solution, calculated as above. As before, we see that we achieve at least 2 digits of accuracy in all cases, and generally more for smaller ε .

TABLE 3.6

Speedup of preconditioned FGMRES to achieve residual stopping tolerance for manufactured solution in (3.5) over direct solution using UMFPACK. In parentheses, the number of digits of accuracy in the preconditioned FGMRES solution.

ε	$N = 2^7$	$N = 2^8$	$N = 2^9$	$N = 2^{10}$	$N = 2^{11}$
10^{-4}	6.81 (3.3)	13.92 (3.0)	18.73 (2.6)	13.03 (3.3)	7.05 (3.6)
10^{-5}	7.75 (5.8)	13.92 (5.5)	27.84 (4.2)	29.68 (4.3)	26.69 (4.0)
10^{-6}	8.04 (4.8)	13.72 (4.4)	19.85 (7.0)	29.02 (6.9)	43.09 (3.8)
10^{-7}	8.33 (3.8)	12.04 (5.9)	18.94 (6.0)	27.64 (5.6)	32.51 (4.6)

4. Conclusions. In this paper, we have extended the ideas of boundary-layer preconditioning for singularly perturbed problems, first proposed for the reaction-diffusion case in [13], to the case of convection-diffusion. As is typically the case, the extension from the symmetric to non-symmetric case requires the development of new tools to extend the theory accordingly, but we are able to provide a sharp bound on the conditioning of the preconditioned system in one dimension, and a weaker bound in two dimensions. Numerical results demonstrate excellent performance of the preconditioner in one and two dimensions, for problems with both exponential and parabolic layers.

In future work, we will consider the extension of these preconditioners to finite-element discretizations of both linear convection-diffusion problems and nonlinear problems with boundary layers, such as Navier-Stokes flow in a channel. We note that while the work presented here focuses on the case of boundary layers, there is

no conceptual restriction that prevents applying the technique to interior layers, so long as the layer structure in the mesh is available for construction of the preconditioner. In the case of non-regular domains or unstructured grids, the regions defined above can be generalized based on whether they include refinement in zero, one, or two dimensions. In regions of no refinement (corresponding to the interior region above), knowledge of node location and convection coefficients can be used to develop a downstream ordering for the Gauss-Seidel approximation. In regions of refinement in one dimension, line relaxation can be generalized based on bin-sorting of geometric coordinates along the non-refined direction. Finally, in regions with refinement in both directions, algebraic multigrid can be used to replace the geometric multigrid used here. While this clearly requires more information than is typically used in global algebraic multigrid approaches, it is feasible given basic information about the geometry, mesh, and coefficients in the PDE.

Another possible direction for future work would be the extension of these techniques to three-dimensional problems. Here, as in the reaction-diffusion case discussed in [13, §5], the number of types of regions in the mesh increases, but no fundamental changes occur in the strategy. Depending on the number of nonzero values in the convection coefficient, a region of the mesh may be of finer resolution in zero, one, two, or three spatial dimensions. The cases of refinement in zero or one dimension are similar to those discussed here, while appropriate plane solves (using multigrid methods appropriate for two dimensions) would be needed for regions with two refined dimensions, and a fully coupled solve (using multigrid methods appropriate for three dimensions) would be needed in any corner regions with three refined dimensions.

REFERENCES

- [1] J. ADLER, S. MACLACHLAN, AND N. MADDEN, *A first-order system Petrov-Galerkin discretisation for a reaction-diffusion problem on a fitted mesh*, IMA J. Numer. Anal., 36 (2016), pp. 1281–1309.
- [2] R. E. ALCOUFFE, A. BRANDT, J. E. DENDY, AND J. W. PAINTER, *The multigrid method for the diffusion equation with strongly discontinuous coefficients*, SIAM J. Sci. Stat. Comput., 2 (1981), pp. 430–454.
- [3] ALI R. ANSARI AND ALAN F. HEGARTY, *A note on iterative methods for solving singularly perturbed problems using non-monotone methods on Shishkin meshes.*, Comput. Methods Appl. Mech. Eng., 192 (2003), pp. 3673–3687.
- [4] ABRAHAM BERMAN AND ROBERT J. PLEMMONS, *Nonnegative Matrices in the Mathematical Sciences*, SIAM, Philadelphia, PA, 1994.
- [5] TIMOTHY A. DAVIS, *Algorithm 832: UMFPACK V4.3—an unsymmetric-pattern multifrontal method*, ACM Trans. Math. Software, 30 (2004), pp. 196–199.
- [6] J. E. DENDY, *Black box multigrid*, J. Comput. Phys., 48 (1982), pp. 366–386.
- [7] CARLOS ECHEVERRÍA, JÖRG LIESEN, DANIEL B. SZYLD, AND PETR TICHÝ, *Convergence of the multiplicative Schwarz method for singularly perturbed convection-diffusion problems discretized on a Shishkin mesh*, Electron. Trans. Numer. Anal., 48 (2018), pp. 40–62.
- [8] PAUL A. FARRELL AND GRIGORII I. SHISHKIN, *On the Convergence of Iterative Methods for Linear Systems arising from Singularly Perturbed Equations*, in Proc. Copper Mountain Conf. on Iterative Methods, 1998, pp. 1–7.
- [9] F. J. GASPAS, C. CLAVERO, AND F. LISBONA, *Some numerical experiments with multigrid methods on Shishkin meshes*, J. Comput. Appl. Math., 138 (2002), pp. 21–35.
- [10] RANDALL J. LEVEQUE, *Finite difference methods for ordinary and partial differential equations*, Society for Industrial and Applied Mathematics (SIAM), Philadelphia, PA, 2007. Steady-state and time-dependent problems.
- [11] R. LIN AND M. STYNES, *A balanced finite element method for singularly perturbed reaction-diffusion problems*, SIAM J. Numer. Anal., 50 (2012), pp. 2729–2743.
- [12] TORSTEN LINSS, *Layer-adapted meshes for reaction-convection-diffusion problems*, vol. 1985 of Lecture Notes in Mathematics, Springer-Verlag, Berlin, 2010.
- [13] S. MACLACHLAN AND N. MADDEN, *Robust solution of singularly perturbed problems using multi-*

- grid methods*, SIAM J. Sci. Comput., 35 (2013), pp. A2225–A2254.
- [14] H. MACMULLEN, E. O’RIORDAN, AND G. I. SHISHKIN, *The convergence of classical Schwarz methods applied to convection-diffusion problems with regular boundary layers*, Appl. Numer. Math., 43 (2002), pp. 297–313.
 - [15] T. P. MATHEW, *Uniform convergence of the Schwarz alternating method for solving singularly perturbed advection-diffusion equations*, SIAM Journal on Numerical Analysis, 35 (1998), pp. 1663–1683.
 - [16] J. J. H. MILLER, E. O’RIORDAN, AND G. I. SHISHKIN, *Fitted numerical methods for singular perturbation problems*, World Scientific Publishing Co. Pte. Ltd., Hackensack, NJ, revised ed., 2012. Error estimates in the maximum norm for linear problems in one and two dimensions.
 - [17] K. W. MORTON, *Numerical solution of convection-diffusion problems*, vol. 12 of Applied Mathematics and Mathematical Computation, Chapman & Hall, London, 1996.
 - [18] T.A. NHAN, S. MACLACHLAN, AND N. MADDEN, *Boundary layer preconditioners for finite-element discretizations of singularly perturbed reaction-diffusion problems*, Numerical Algorithms, 79 (2018), pp. 281–310.
 - [19] THÁI ANH NHAN, MARTIN STYNES, AND RELJA VULANOVIĆ, *Optimal uniform-convergence results for convection–diffusion problems in one dimension using preconditioning*, Journal of Computational and Applied Mathematics, 338 (2018), pp. 227 – 238.
 - [20] THÁI ANH NHAN AND RELJA VULANOVIĆ, *Analysis of the truncation error and barrier-function technique for a Bakhvalov-type mesh*, Electron. Trans. Numer. Anal., 51 (2019), pp. 315–330.
 - [21] HANS-GÖRG ROOS, *A note on the conditioning of upwind schemes on shishkin meshes*, IMA Journal of Numerical Analysis, 16 (1996), pp. 529–538.
 - [22] HANS-GÖRG ROOS, MARTIN STYNES, AND LUTZ TOBISKA, *Robust numerical methods for singularly perturbed differential equations*, vol. 24 of Springer Series in Computational Mathematics, Springer-Verlag, Berlin, second ed., 2008.
 - [23] Y. SAAD, *Iterative methods for sparse linear systems*, Society for Industrial and Applied Mathematics, Philadelphia, PA, second ed., 2003.
 - [24] MARTIN STYNES AND DAVID STYNES, *Convection-diffusion problems*, vol. 196 of Graduate Studies in Mathematics, American Mathematical Society, Providence, RI, 2018.
 - [25] R. S. VARGA, *Matrix Iterative Analysis*, Springer Series in Computational Mathematics, Springer, Berlin, 2000. Second Edition.
 - [26] HOMER F. WALKER, *Implementation of the GMRES method using Householder transformations*, SIAM J. Sci. Statist. Comput., 9 (1988), pp. 152–163.